Boundary Layer Transition in Mach 4 Flow with Varying Angle of Attack

Catherine M. Stock[1] and Dr. Stuart J. Laurence[2]
University of Maryland, College Park, MD, 20742, United States

Boundary layer transition in hypersonic flow is often studied at Mach numbers above 4, where second mode instabilities are known to drive the breakdown from laminar to turbulent flow. At Mach 4, however, these second mode disturbances are weaker, and transition may instead be influenced by first mode or mixed instability mechanisms. Because of this, transition behavior in the Mach 4 regime is less clearly understood, especially under varying angle of attack conditions. To investigate this, Mach 4 flow over a sharp nose cone was studied in the University of Maryland Multi-phase Investigations Supersonic Tunnel (MIST) Ludwieg tube using high speed Schlieren imaging. Several test cases with varying angle of attack and fill pressure were analyzed using Spectral Proper Orthogonal Decomposition (SPOD) to identify the dominant coherent disturbances and examine their downstream development. Transition onset was estimated from rapid increases in modal amplitude and energy, indicating a later transition at more negative angles of attack and an earlier transition at more positive angles of attack. Transitional cases showed dominant instability frequencies between approximately 31 and 49 kHz. These results provide additional insight into boundary layer transition in Mach 4 flow.

Introduction

The transition of a hypersonic boundary layer from laminar to turbulent flow leads to major increases in drag, surface heating, and flow separation. Because of this, understanding when and why boundary layer transition occurs over a body in hypersonic flow is a vital part of hypersonic vehicle design. If laminar flow can be maintained over more of the vehicle surface, both aerodynamic heating and drag can be reduced.[1]

Classical linear stability theory states that compressible boundary layers support multiple unstable modal disturbances. Boundary layer transition is typically described as sequential flow disturbance generation, linear growth of those disturbances, and their eventual nonlinear breakdown into turbulence. At lower compressible speeds, first mode instabilities are dominant. At higher Mach numbers, in the hypersonic regime, a high frequency acoustic disturbance known as the second mode typically becomes dominant. [2] Much of existing boundary layer transition research has focused on flows above Mach 4, where second mode waves dominate.

The Mach 4 regime, however, is not as straightforward. In this regime, second mode disturbances are generally weaker than they are in higher Mach number flows, and first mode or mixed mode mechanisms play a large role in the transition process. This means that conclusions drawn from studies from Mach 10 to Mach 14 cannot always be directly applied to Mach 4 conditions. In particular, there is still limited experimental data showing how parameters such as angle of attack affect instability growth and transition onset at Mach 4.

Recent work using high speed Schlieren imaging and spectral analysis has shown how valuable optical diagnostics can be for studying boundary layer instabilities. Kennedy and Laurence, for example, used time resolved Schlieren imaging to capture second mode wave growth over a cone in Mach 14 flow in the Arnold Engineering Development Complex (AEDC) Tunnel 9 facilities. Their results showed how coherent disturbances amplified downstream before breaking down into turbulence. While studies like this have greatly improved the understanding of high Mach number transition, similar investigations at Mach 4 are much less common.[3] Therefore, it is important to study the identification of coherent structures and track their spatial growth to understand transition onset in this regime.

The present work helps address that gap by studying boundary layer transition over a sharp cone in Mach 4 flow under varying angles of attack. High-speed Schlieren imaging was used to capture the unsteady flow field, and

[1] Undergraduate Student, Department of Aerospace Engineering, and AIAA Student Member.
[2] Associate Professor, Department of Aerospace Engineering, and AIAA Senior Member.

Spectral Proper Orthogonal Decomposition (SPOD) was applied to extract the dominant coherent disturbances from the image data. Unlike point based measurements, SPOD makes it possible to examine how these structures evolve across the flow field in view. Using this approach, dominant instability frequencies, reconstructed mode shapes, disturbance growth rates, and energy amplification metrics were compared across various test conditions.

I. Methodology

A. Data Collection

All experiments were conducted in the MIST Mach-4 Ludwieg tube at The University of Maryland, College Park in the High Speed Aerodynamics and Propulsion Laboratory. The tunnel is made up of four sections: a high-pressure charge tube, a converging-diverging nozzle, a free jet test section, and an unheated charge tube. The nozzle is axisymmetric and designed with a throat and exit radii of 3.16 cm and 10.44 cm, respectively, to produce Mach 4 flow in the test section.[4] Within the tunnel, a sharp nose cone test article was mounted in the free jet test section. The flow exiting the converging-diverging nozzle moves at Mach 4 and flows through the test section. The characteristics of this flow over the body are captured by high-speed cameras.

This study investigates the influence of angle of attack on boundary layer transition behavior over the sharp nose cone. A total of six experimental shots were analyzed, with the angle of attack varying between -2.35 degrees and 2.65 degrees, and fill pressures ranging from 70 kPa to 350 kPa. The variation in freestream conditions altered the Reynolds number of the flow, but allowed for both laminar and turbulent regimes to be observed over the nose cone at particular angles of attack. At lower angles of attack, the fill pressure needed to be higher to achieve transition, and at higher angles of attack, the fill pressure needed to be lower. This change of the fill pressure slightly changes the freestream Mach number. Previous facility characterization showed that for fill pressures below 100 kPa, the freestream Mach number, M_∞, decreases below the nominal Mach 4 condition, ranging from approximately 3.75 to 3.9 for 50–90 kPa. For fill pressures above 100 kPa, the core-flow freestream Mach number approaches $M_\infty \approx 4$. Therefore, the lower-pressure cases in the present study may have slightly lower Mach number than the higher-pressure cases, in addition to having a lower unit Reynolds number. A summary of the test conditions and initial observations regarding laminar to turbulent transition is provided in Table 1.

Table 1 Test Conditions

Shot	Angle of Attack (degrees)	Fill Pressure (kPa)	Re_∞ (m^{-1})	Transitional?
A-2.35Re16	-2.35	350	16.4e6	Yes
A-1.7Re13	-1.7	275	12.9e6	Yes
A-0.7Re10	-0.7	215	10.1e6	Yes
A0.6Re4.7	0.6	100	4.68e6	Yes
A1.7Re3.3	1.7	70	3.28e6	Yes
A2.65Re3.3	2.65	70	3.28e6	Turbulent

Schlieren imaging techniques were used to view the boundary layer over the surface of the cone model. The setup was a standard Z-typer horizontal knife-edge Schlieren. For high-speed imaging, a Phantom TMX 7510 camera was used. The camera and all other equipment was mounted on either side of the test section, with the camera aligned with the cone's upper surface. The Schlieren images were set to have a resolution of 1280x96 pixels and a framerate of 610 kHz. Based on the model and spacing, the scale factor of the images is then 0.077 mm/pixel.

B. Image Processing

The Schlieren images taken for each test run were processed prior to detecting the boundary layer transition. For each experimental run, 2,000 subsequent frames were extracted after the chosen starting frame from the full video sequence, corresponding to around 3,200 microseconds of flow time to be analyzed.

Each frame was then cropped to remove regions of no physical interest. The intensity at each pixel is then averaged across each frame. The average intensity of each pixel then creates a mean image that is representative of the steady background signal in the data set. This mean image is then subtracted from each individual frame in the set, effectively removing stationary features and background noise. The resulting image enhances the visibility of the flow structures.

This preprocessing step is important prior to boundary layer transition detection because SPOD analyzes the structure of flow fluctuations in the frequency domain. By removing the mean image, the dataset is normalized,

ensuring that SPOD captures only the dynamically relevant features rather than any experimental noise and other artifacts. Without processing, the SPOD results could be dominated by low frequency non physical intensity fluctuations.

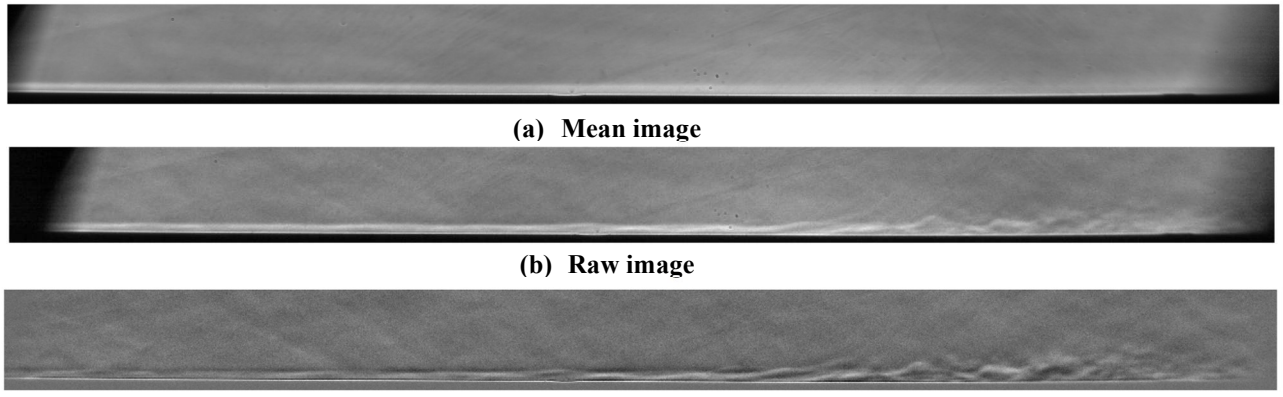

(a) Mean image

(b) Raw image

(c) Processed Image

Fig. 1: Shot A-0.7Re10, frame one

C. Spectral Orthogonal Decomposition

Manually identifying flow structures and indicating their breakdown is time consuming and difficult. Spectral Orthogonal Decomposition is a method of empirically extracting structures from flow. The analysis was performed using the spectral proper orthogonal decomposition (SPOD) MATLAB package developed by Towne et al., which enables frequency modal decomposition of unsteady flow fields.[5]

The input for the SPOD algorithm consists of the preprocessed images described above. Each data set had a sampling frequency of 610 kHz, making the time step between consecutive images 1.63 microseconds. A Hamming window length of 1,000 was used within the SPOD process. SPOD utilizes windowing techniques to minimize the reduction of peak amplitudes by artificially rendering the data in each temporal block.[5]

The decomposition yields eigenvalues $\lambda(f)$, representing modal energy as a function of frequency, and eigenfunctions corresponding to coherent flow structures. The SPOD spectrum was constructed by plotting the leading eigenvalue $\lambda_1(f)$, corresponding to SPOD first mode, versus the frequency on a logarithmic scale, as seen in Figure 2.

To better understand the dominant instability structures, the SPOD mode shape associated with selected frequencies was reconstructed using the complex eigenfunction and its harmonic time dependence. These reconstructed fields were plotted in axial and radial coordinates with color contours representing disturbance intensity. This makes it possible to directly visualize how the coherent fluctuations are organized within the boundary layer region. Figure 2 shows that the peak modal energy in the SPOD spectrum extends from 30 kHz to 80 kHz. As seen in Figure 3, the SPOD first mode reconstruction for Shot A-0.7Re10 starts to develop and become clear around 40kHz, and at higher frequencies, the structure starts to break down. Because of this observation, the relevant frequency band to search for frequency peaks was 30 kHz to 80kHz. The dominant instability frequency within this band for each shot was identified as the peak in this spectrum. A summary of the corresponding peak frequency for each shot is shown in Table 2.

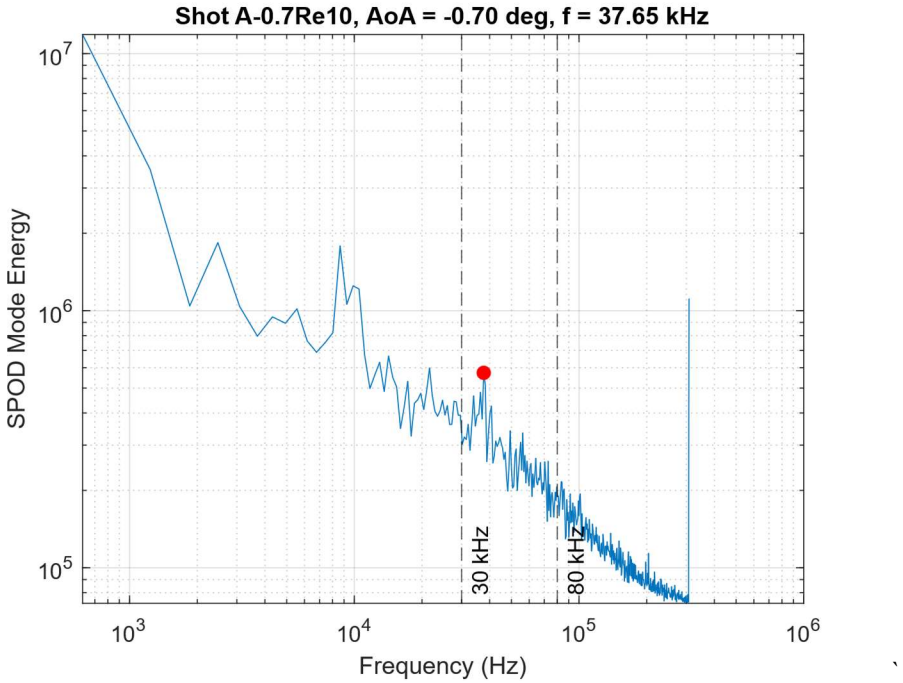

Fig. 2: Shot A-0.7Re10 SPOD spectrum with the indicated peak frequency

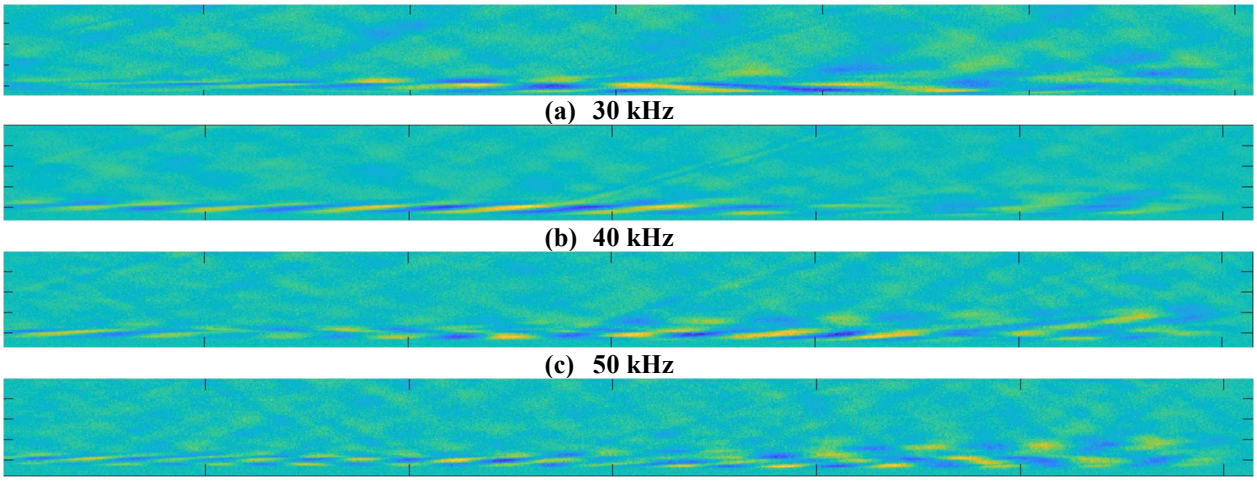

(a) 30 kHz

(b) 40 kHz

(c) 50 kHz

(d) 60 kHz

Fig. 3: Shot A-0.7Re10 SPOD mode one at increasing frequencies

Table 2 Peak Frequencies

Shot	Peak Frequency (kHz)
A-2.35Re16	49
A-1.7Re13	47
A-0.7Re10	37
A0.6Re4.7	34
A1.7Re3.3	33
A2.65Re3.3	31

D. Analysis

Following the SPOD implementation, additional post processing was performed to quantify the streamwise amplification of the dominant instability structure and estimate the onset of boundary layer transition. The objective of this analysis was to track the spatial growth of the most energetic coherent disturbance identified by SPOD and compare amplification behavior across test conditions.

For each shot, the dominant frequency was selected from the leading SPOD eigenvalue spectrum as the peak within the band of frequencies relevant to instability. The corresponding complex SPOD mode shape was then extracted from the eigenfunction matrix P.

To obtain a one dimensional measure of disturbance amplitude, the wall normal root mean square (RMS) magnitude of the complex mode shape was computed at each streamwise location:

$$A(x) = \sqrt{\frac{1}{N_y}\sum_{j=1}^{N_y} |\phi(x, y_j)|^2} \tag{1}$$

where $\phi(x, y)$is the selected SPOD mode shape and N_y is the number of wall normal pixels in the cropped Schlieren field of view. This operation collapses the two dimensional modal structure into a streamwise amplitude envelope representing the local disturbance strength. A moving average filter was then applied to the streamwise amplitude to reduce pixel-scale noise and improve the robustness of the growth estimates.

The spatial amplification rate of the disturbance was evaluated using the streamwise derivative of the smoothed amplitude distribution, which provides a direct measure of how rapidly instability grows downstream. For comparison between shots, the derivative was normalized by its maximum absolute value. The transition location was estimated as the point of maximum positive growth beyond an upstream buffer region. This criterion identifies the location where rapid modal amplification begins, corresponding to the onset of laminar breakdown.

To quantify disturbance amplification in a form analogous to classical linear stability theory, an e^N metric was also computed. The disturbance energy was defined as

$$E(x) = A(x)^2 \tag{2}$$

and referenced to the average upstream energy E_0 over the initial portion of the image sequence. The local N-factor was then calculated as

$$N(x) = \frac{1}{2}\ln\left(\frac{E(x)}{E_0}\right) \tag{3}$$

where $N(x)$ represents the logarithmic growth of disturbance amplitude relative to the upstream reference state. The maximum value of N and the slope of the approximately linear growth region were used as a comparative indicator of instability amplification strength.

Within each experimental shot, three primary metrics were extracted: peak frequency, growth slope, and transition location (x_{tr}). These quantities were then compared to evaluate the behavior of the development of boundary layer transition in Mach 4 flow.

II. Results and Discussion

The reconstructed modes for shot A-0.7Re10 are shown in Figure 3 at frequencies of 37, 40, 50, and 60 kHz. These frequencies were selected to examine how the leading disturbance changes across the energetic portion of the spectrum. At the lower frequencies, the mode appears as a longer and more continuous wave structure that extends downstream. As the frequency increases, the disturbance becomes shorter in wavelength and less uniform.

This behavior is important because it reflects the progression of boundary layer transition. At lower frequencies, the reconstructions capture coherent instability waves associated with the growth of a dominant disturbance. As frequency increases, the flow exhibits less organized structure, indicating the breakdown of this dominant peak into a broader spectrum of disturbances. These higher-frequency modes therefore represent the early stages of transition, where the flow loses coherence and evolves toward turbulence.

Figure 3, therefore, provides an important connection between the SPOD spectrum and the transition metrics developed later in the analysis. While the spectrum identifies where energetic disturbances occur in frequency space, the reconstructed modes show how those disturbances physically evolve within the boundary layer. Together, these results indicate that Mach 4 transition is associated not only with the presence of a dominant frequency peak, but also with the progressive loss of coherence of the underlying instability structures.

The variation of the dominant SPOD frequency with angle of attack is shown in Figure 3. The data shows a clear inverse relationship between angle of attack and dominant SPOD frequency, with peak frequency decreasing from about 49 kHz at negative angles to roughly 31 kHz at positive angles. This trend indicates a shift from shorter-wavelength, higher-frequency disturbances to longer-wavelength, lower-frequency structures as the angle of attack increases

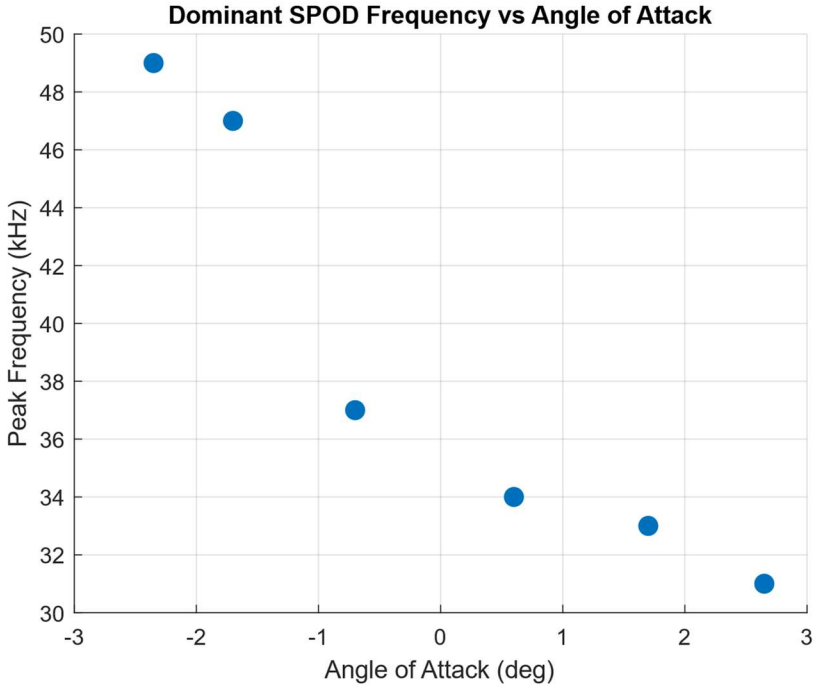

Fig. 3: Angle of Attack vs Peak Frequency

The quantitative analysis results for all six test cases are summarized in Table 3. For each shot, the streamwise transition location from the tip of the nose cone, maximum modal amplitude, growth slope, and maximum N-factor were extracted from the dominant SPOD mode. These quantities provide a basis for comparing instability amplification and transition behavior across the range of test conditions.

Table 3 Analysis Results

Shot	Re_∞ (m^{-1})	AoA (deg.)	x_{tr} (mm)	Re_{tr}	Max Amplitude	Growth Slope	Max N
A-2.35Re16	16.4e6	-2.35	307.7	5.0e6	3.91e-3	1.65e-06	0.937
A-1.7Re13	12.9e6	-1.7	288.8	3.7e6	4.53e-3	2.70e-06	1.23
A-0.7Re10	10.1e6	-0.7	278.5	2.8e6	4.73e-3	3.63e-06	1.37
A0.6Re4.7	4.68e6	0.6	300.1	1.4e6	3.67e-3	1.99e-06	0.600
A1.7Re3.3	3.28e6	1.7	289.1	0.95e6	4.15e-3	1.93e-06	0.919
A2.65Re3.3	3.28e6	2.65	239.9	0.78e6	3.86e-3	NaN	0.935

The influence of angle of attack on transition location cannot be fairly deduced from transition distance from the tip alone, as various tunnel operating conditions were used. At the same unit Reynolds number of 3.28×10^6, increasing the angle of attack from 1.7° to 2.65° moves the transition location from 289.1 mm to 239.9 mm. This follows behavior that is well established in hypersonic boundary layer theory, with a higher angle of attack resulting in earlier boundary layer transition.

To compare across all cases regardless of Reynolds number, the transition Reynolds number was defined as $Re_{tr} = Re_\infty x_{tr}$. The resulting values show a clear dependence on angle of attack, as seen in Figure 4. As the angle of attack increases in the positive direction, the transition Reynolds number decreases. The most negative angle of attack

corresponds to the highest transition Reynolds number, while the largest positive angle of attack yields the lowest value. This trend indicated that transition occurs under lower accumulated instability growth at higher angles of attack and greater accumulated instability growth at lower angles of attack. The decrease in transition Reynolds number with increasing angle of attack indicates that transition occurs after less streamwise development of the boundary layer, demonstrating that higher angles of attack promote earlier transition.

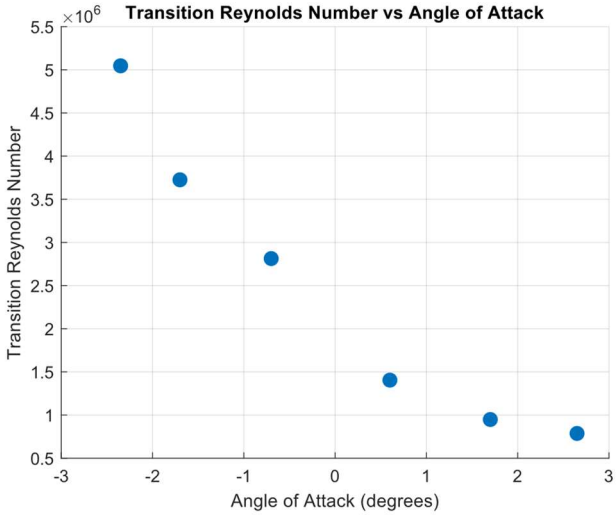

Fig. 4 Transition Reynolds Number vs Angle of Attack

Among the transitional cases, the measured growth slope showed a clear relationship with transition location. The earliest transition location was 239.9 mm from the tip of the cone for shot A2.65Re3.3, which was observed to be mostly turbulent, and a growth slope could not be calculated. Shot A-0.7Re10 had the largest growth slope, 3.63×10^{-6}, and the earliest transition locations of the observably transitional shots at 278.5 mm. Similarly, shot A-1.7Re13 showed the second largest growth slope, 2.70×10^{-6}, with transition occurring at 288.8 mm, the second latest transition. By comparison, shot A-2.35Re16 had the smallest measured growth slope, 1.65×10^{-6}, and the latest transition location at 307.7 mm. This trend suggests that stronger disturbance amplification leads to earlier breakdown of the boundary layer, consistent with classical stability theory.

The N-factor values reported in Table 3 remain relatively low, ranging from 0.6 to 1.37, which is consistent with the flow being in the early stages of transition. In general, higher N-factors correspond to greater amplification of disturbances, and the largest values observed here tend to align with cases that also exhibit higher growth slopes and amplitudes. However, the overall variation in N across the dataset is modest, and no clear trend with either Reynolds number or angle of attack is evident.

It is important to note that the N-factor values reported here are based on measurements taken over a limited spatial region. As a result, they may not capture the full disturbance growth history. It is likely that a portion of the amplification occurred upstream of the measurement window, meaning that the initial disturbance energy and early growth stages are not fully accounted for. This makes it difficult to directly compare N-factors across cases or to draw strong conclusions about their dependence on flow conditions.

III. Conclusions

This study investigated boundary layer transition over a sharp cone in Mach 4 flow using high-speed Schlieren imaging and SPOD. The objective was to examine how varying angles of attack and fill pressure influenced instability growth and transition onset, and to demonstrate the usefulness of SPOD as a tool for extracting coherent disturbance structures from time-resolved optical data. The results show that transition is accompanied by a clear evolution in disturbance structure, where low-frequency modes appear as coherent, elongated waves and higher-frequency modes become shorter, less uniform, and increasingly disordered. This progression reflects the breakdown of a dominant instability into a broader spectrum of disturbances, linking the SPOD spectrum directly to the physical transition process.

A relationship was observed between angle of attack, dominant frequency, and transition Reynolds number. Increasing the angle of attack shifts the dominant SPOD frequency to lower values while simultaneously decreasing

the transition Reynolds number. The reduction in Re_{tr} indicates that transition occurs after less accumulated instability growth, demonstrating that disturbances amplify more rapidly at higher angles of attack. The associated shift to lower frequencies suggests that the dominant instability is characterized by longer-wavelength structures under these conditions. Conversely, negative angles of attack correspond to higher-frequency, shorter-wavelength disturbances and higher transition Reynolds numbers. These trends confirm that angle of attack plays a primary role in setting the spectral content of the instability and the amplification of disturbances before transition occurs.

Overall, this work demonstrates that SPOD provides an effective framework for analyzing hypersonic boundary layer transition using Schlieren imaging. By linking dominant frequencies, spatial mode structures, and growth behavior, the method captures both the spectral and physical evolution of instability waves. Future work should focus on independently varying angle of attack and Reynolds number to better isolate their individual effects, as well as comparing the observed disturbances with linear stability theory to determine whether the dominant mechanisms correspond to first-mode, second-mode, or mixed-mode instabilities.

Acknowledgments

I would like to thank Dr. Stuart Laurence for his invaluable guidance during my time in the Aerospace Honors Program. I would also like to thank Ryan Di Silva and Travis Duchene for their assistance on my project.

Appendix

A. SPOD Spectrum Plots

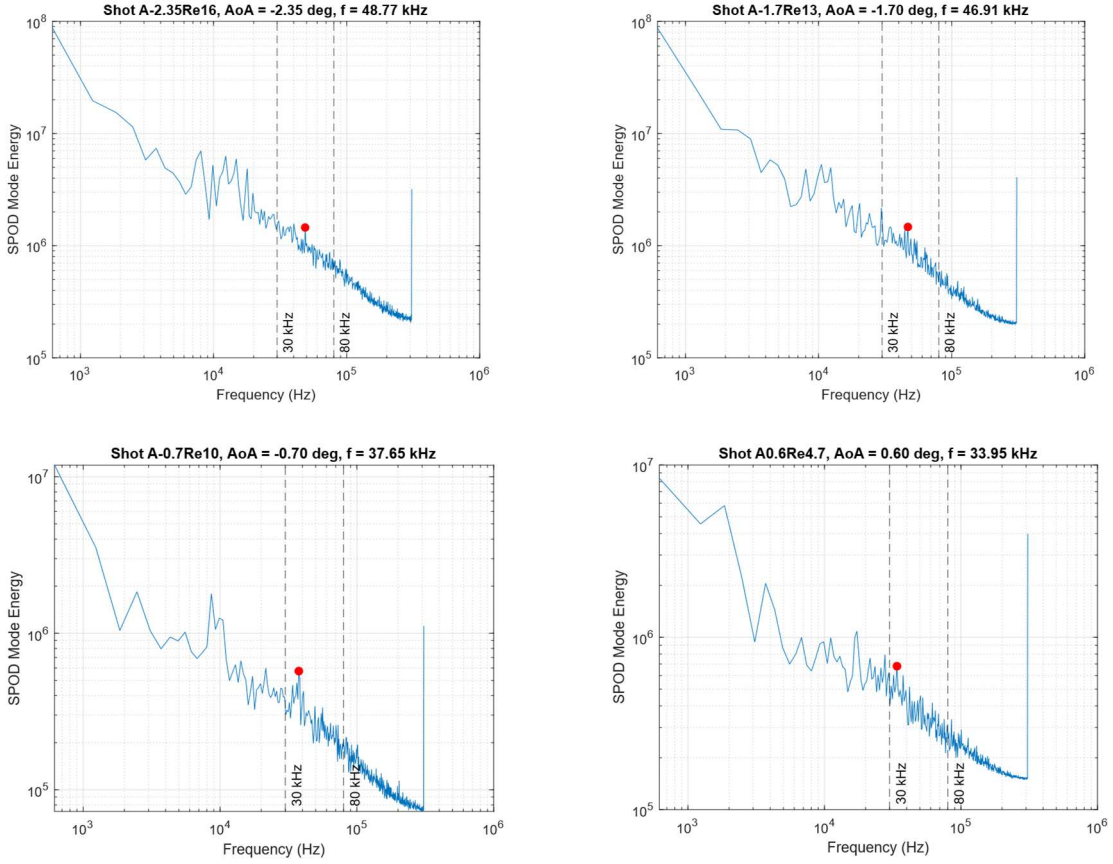

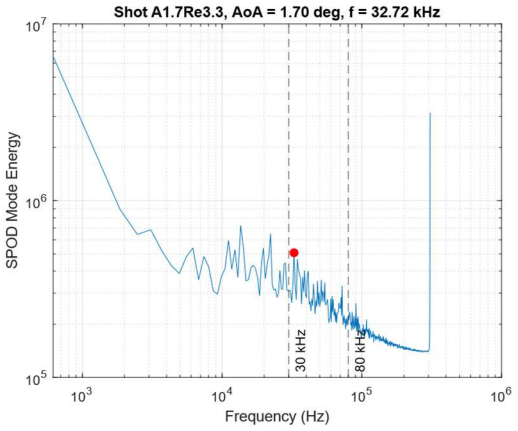

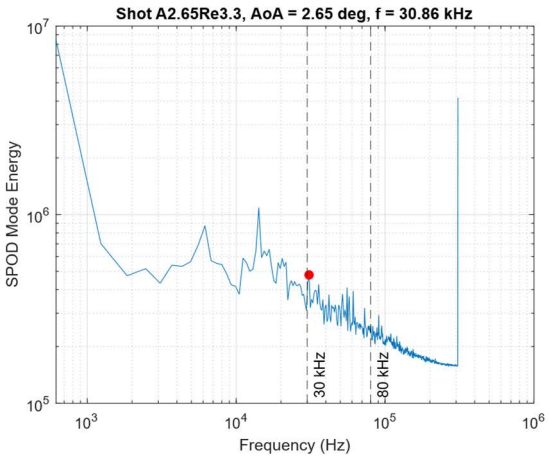

B. Transition Detection Graphs

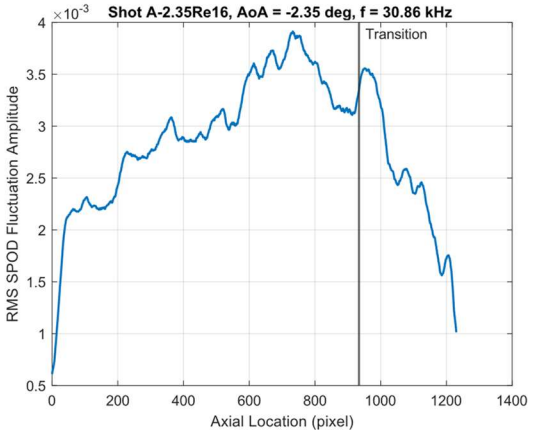

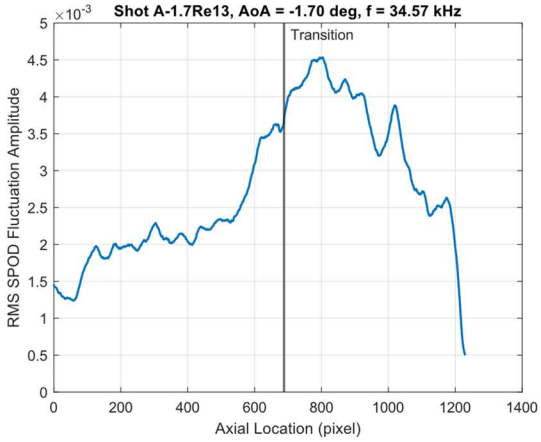

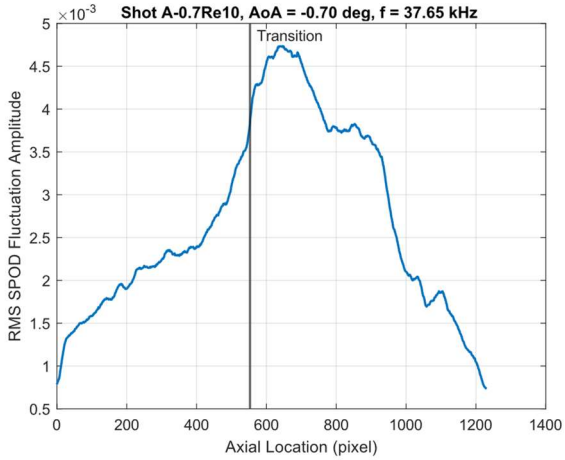

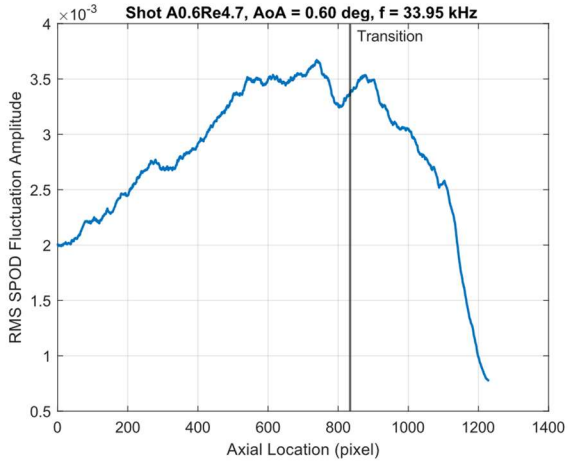

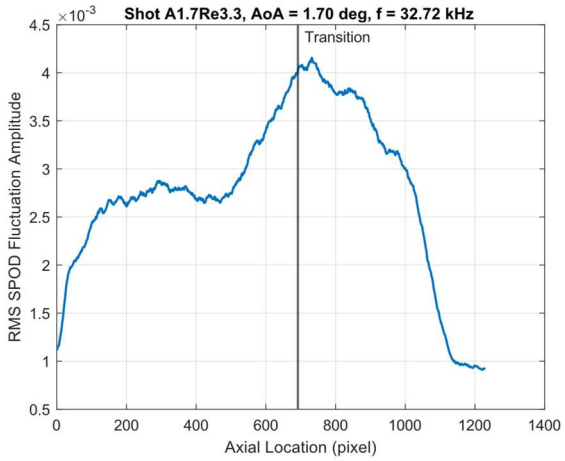

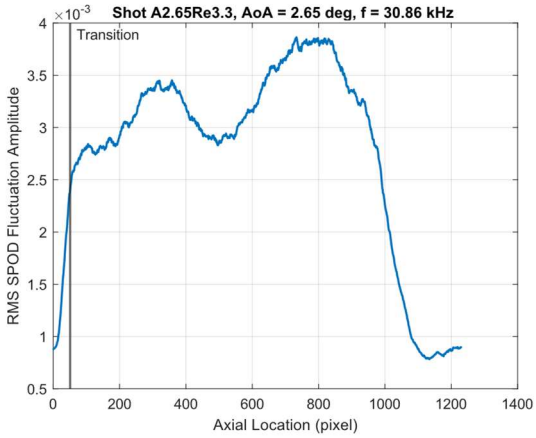

References

1. Swanson, E. O., "Boundary-Layer Transition on Cones at Angle of Attack in a Mach-6 Quiet Tunnel," Ph.D. Dissertation, Purdue University, West Lafayette, IN, 2008. (docs.lib.purdue.edu)
2. Mack, L. M., "On the Application of Linear Stability Theory to the Problem of Supersonic Boundary-Layer Transition," *AIAA 12th Aerospace Sciences Meeting*, AIAA Paper 74-134, Washington, DC, Jan. 1974. (ntrs.nasa.gov)
3. Kennedy, R. E., Laurence, S. J., Smith, M. S., and Marineau, E. C., "Visualization of the Second-Mode Instability on a Sharp Cone at Mach 14," *2018 AIAA Aerospace Sciences Meeting*, AIAA Paper 2018-2083, Kissimmee, FL, Jan. 2018. https://doi.org/10.2514/6.2018-2083 (arc.aiaa.org)
4. Laurence, S. J., and Schoneich, M., "Development of a Supersonic Ludwieg-Tube Facility for Investigating High-Speed Multi-Phase Flows," *AIAA SCITECH 2024 Forum*, AIAA Paper 2024-2083, 2024. https://doi.org/10.2514/6.2024-2083
5. Towne, A., Schmidt, O. T., and Colonius, T., "Spectral Proper Orthogonal Decomposition and Its Relationship to Dynamic Mode Decomposition and Resolvent Analysis," *Journal of Fluid Mechanics*, Vol. 847, 2018, pp. 821–867. https://doi.org/10.1017/jfm.2018.283